The Meteoritical Society

Meteoritics & Planetary Science 50, Nr 8, 1378–1391 (2015)
doi: 10.1111/maps.12474

Survival of refractory presolar grain analogs during Stardust-like impact into Al foils: Implications for Wild 2 presolar grain abundances and study of the cometary fine fraction

T. K. CROAT[1,*], C. FLOSS[1], B. A. HAAS[1], M. J. BURCHELL[2], and A. T. KEARSLEY[2,3]

[1]Laboratory for Space Sciences and Department of Physics, Washington University, St. Louis, Missouri 63130, USA
[2]Centre for Astrophysics and Planetary Science, School of Physical Sciences, University of Kent, Canterbury CT2 7NH, UK
[3]Department of Earth Sciences, Natural History Museum, London SW7 5BD, UK
[*]Corresponding author. E-mail: tkc@wustl.edu

(Received 02 February 2015; revision accepted 04 May 2015)

Abstract–We present results of FIB–TEM studies of 12 Stardust analog Al foil craters which were created by firing refractory Si and Ti carbide and nitride grains into Al foils at 6.05 km s^{-1} with a light-gas gun to simulate capture of cometary grains by the Stardust mission. These foils were prepared primarily to understand the low presolar grain abundances (both SiC and silicates) measured by SIMS in Stardust Al foil samples. Our results demonstrate the intact survival of submicron SiC, TiC, TiN, and less-refractory Si_3N_4 grains. In small (<2 μm) craters that are formed by single grain impacts, the entire impacting crystalline grain is often preserved intact with minimal modification. While they also survive in crystalline form, grains at the bottom of larger craters (>5 μm) are typically fragmented and are somewhat flattened in the direction of impact due to partial melting and/or plastic deformation. The low presolar grain abundance estimates derived from SIMS measurements of large craters (mostly >50 μm) likely result from greater modification of these impactors (i.e., melting and isotopic dilution), due to higher peak temperatures/pressures in these crater impacts. The better survivability of grains in smaller craters suggests that more accurate presolar grain estimates may be achievable through measurement of such craters. It also suggests small craters can provide a complementary method of study of the Wild 2 fine fraction, especially for refractory CAI-like minerals.

INTRODUCTION

The NASA Stardust mission captured and returned samples from comet Wild 2, allowing the first laboratory analyses of unambiguous cometary material. Contrary to many expectations for material from the outer solar system, the samples did not consist entirely of primitive matter similar to chondritic porous interplanetary dust particles (IDPs), but rather contained high temperature minerals and fragments of CAIs and chondrules indicative of formation in the inner solar system (Brownlee et al. 2006, 2012). Presolar grain abundances, which are a good indicator of the degree to which a given sample has preserved the original starting material from the solar nebula, were considerably lower than expected (McKeegan et al. 2006; Stadermann et al. 2008). These and other results from the Stardust mission have changed our conception of the distribution and transport of matter in the early solar system.

The study of Stardust cometary materials is complicated by the unavoidable degradation of the samples upon capture at 6.1 km s^{-1}, during the fly-by through the cometary coma. While many coarse grains (>5 μm) were largely preserved in aerogel as terminal particles, the fine fraction of cometary material was significantly degraded. Aggregates of this fine fraction are believed to have created the bulbous Type B and Type C tracks (Hörz et al. 2006; Burchell et al. 2008a; Trigo-Rodríguez et al. 2008), which was recently confirmed in the analog experiments of Kearsley et al. (2012). Unfortunately, the captured fine material

becomes intimately mixed with melted aerogel along the track walls, which greatly complicates its analysis and interpretation. Efforts are underway to compress and concentrate surviving fine grains from bulbous tracks, but initial results suggest that many grains melted on impact (Stodolna et al. 2012; Brownlee et al. 2013). The study of small craters in Al foil offers a complementary approach for understanding the cometary fine fraction (Kearsley et al. 2009; Croat et al. 2013, 2014). In these craters, the fine material is concentrated and localized, allowing one to determine bulk compositions and to infer the initial grain sizes, although internal grain textures may have been modified or destroyed by relatively high shock pressures (Wozniakiewicz et al. 2009, 2012a, 2012b).

Other limitations of the Stardust samples have become apparent in the course of presolar grain abundance determinations. Here, measurements were focused primarily on the Al foil-captured cometary samples as these presented concentrated targets for isotopic measurement, and in particular on larger craters that enable measurement of sufficient area to more quickly reach statistical significance. During the preliminary NanoSIMS examination, only a single presolar grain was found (on the raised rim at the edge of an Al crater), leading to initial estimates of an ~8 ppm O-rich presolar grain abundance for Wild 2 (McKeegan et al. 2006; Stadermann et al. 2008), far lower than the 150–200 ppm levels in primitive meteorites and ≥375 ppm level in primitive chondritic porous IDPs (Floss et al. [2013] and references therein). Given the violent capture method, the possibility that presolar grains are destroyed or altered during capture in a way that prevents detection of their isotopic anomalies must be considered.

Our knowledge of the sample degradation that occurs on capture has been greatly aided by the study of Stardust analogs produced by hypervelocity impact experiments (e.g., Kearsley et al. 2006, 2007, 2008; Wozniakiewicz et al. 2009, 2012a, 2012b). Using light-gas guns (LGG), well-characterized grains can be fired into the Stardust capture media (aerogel tiles and Al foils) at velocities of 6 km s^{-1}, thus simulating the Stardust encounter (Burchell et al. 1999). These samples can then be studied for alteration and/or degradation during capture of the materials of interest, which can then be applied to interpretation of the Stardust samples. For example, recent hypervelocity impact experiments were made using primitive meteorite matrix material, which is dominated by fine-grained mafic silicate species and which has high presolar grain abundances (Acfer 094 with ≈80 ppm oxide and silicates and ≈15 ppm SiC; Floss et al. [2013]). After capture in Al foil, the material showed ~20× and ~3× reductions in the presolar grain abundances of oxides/silicates and SiC, respectively, indicating considerable destruction and/or modifications of these grains on impact. Applying the correction factors derived from these experiments to the earlier Stardust measurements leads to revised Wild 2 presolar silicate and oxide abundances of 600–800 ppm (Floss et al. 2013), similar to the range observed in IDPs and other primitive solar system materials.

Here, we present further studies of Stardust analog samples, with a primary focus on FIB–TEM investigations of the condition and survival of small (mostly <1 μm) refractory mineral grains (including SiC) within Al foil craters. These are intended to better understand the modification of submicron grains upon capture and to clarify the possible causes of the lower measured presolar grain abundances in the Acfer 094 analog sample and the Wild 2 samples. Preliminary results were reported by Croat et al. (2013, 2014).

SAMPLES AND EXPERIMENTAL METHODS

The analog grains chosen for this hypervelocity impact experiment were crystalline refractory phases mostly submicron in size, including natural diamond, synthetic TiN, synthetic TiC, synthetic SiC, synthetic alumina (Al_2O_3), synthetic Si_3N_4, and natural olivine ($Fo_{90}Fa_{10}$) with approximate melting temperatures of 3550, 3160, 2930, 2730, 2070, 1900, and 1830 °C, respectively. Size distributions were determined for SiC, Si_3N_4, TiC, and TiN projectile grains using TEM imaging; the median grain sizes were 500–700 nm, with diameters ranging from 100 nm up to several μm. As the peak of the presolar SiC size distribution is ~500 nm (Daulton et al. 2003), these synthetic SiC grains are good analogs for presolar SiCs. The mineral grains were faceted crystals (ellipticity of 1.4 ± 0.4 for all grain populations) with crystal structures that match the expected phases (i.e., TiC: a = 4.35Å [fcc]; TiN: a = 4.25Å [fcc]; SiC, a = 4.35Å [fcc]; Si_3N_4 a = 7.8Å, c = 5.6 Å [trigonal]). This mixture of refractory minerals was then cemented together with polyvinyl acetate (PVA) to create ~100 μm and larger sized aggregate projectiles of suitable size for firing. These were then shot at normal incidence into flight spare Al 1100 foil (identical to that used in the Stardust mission) using the two stage LGG at the University of Kent (Burchell et al. 1999). The impact speed of this shot (named G070809#2) was 6.05 km s^{-1}, comparable to the capture speed of Wild 2 cometary particles. From previous experiments (e.g., Kearsley et al. 2009), it is known that weaker aggregate projectiles may fragment in the LGG, resulting in impacts by a wide range of particle sizes, including many of the separated subgrain components.

SEM images and energy dispersive X-ray (EDX) spectra, which give the average compositions at the bottoms of craters, were collected from all craters (N = 1350) within two randomly selected 1.8 by 1.3 mm areas of the cratered Al foil. Spectral images which collect a full X-ray spectrum for each pixel were also acquired from ~50 craters, allowing X-ray composition maps to be generated (2000–5000× magnification; 256x256 pixels; ~30 min acquisition; using Noran System 7 software). Geometrical effects may restrict the collection of analytical data from surviving material which is concentrated at the bottom of craters (Kearsley et al. 2007), so for this study, the X-ray collection was optimized by tilting the sample toward the detector by 10°. All spectra are dominated by an Al peak, but ~80% also contain other elements that emanate from surviving projectile material. In this work, we concentrate on the half of the craters (N = 758) that were dominated by Ti or Si, that is, those created by impact of the Ti, Si carbides and nitrides that are the best analog materials for presolar SiC. Olivine and corundum results are not presented here; the olivine analog grains (of ~8 μm diameter) and their resulting craters were too large to allow comparison with fine-grained olivines, and any surviving corundum Al_2O_3 grains were disguised by the large Al peak from the foil. The median diameters of the Ti-rich and Si-rich crater populations were 2.0 and 1.5 μm, respectively, which is consistent with craters forming from impacts of individual crystallites rather than larger aggregates (assuming the projectile-to-crater size relationships established by Kearsley et al. [2006] and Price et al. [2010]). Thus, we conclude that some mm-sized projectiles did fragment into the various ~1 μm-sized constituent grains upon firing. Most (~85%) of the Ti- or Si-rich spectra showed only Ti or Si, but not both, again suggesting the projectile material fragmented into single grain impactors (of TiN, SiN, SiC, or Si_3N_4) during the firing process.

Electron transparent cross sections of eight Ti-rich and four Si-rich craters were prepared using the focused ion beam (FIB) lift-out technique with an FEI Quanta 3-D instrument. The craters were selected so as to sample the overall crater population, with a range of size and Ti or Si X-ray count rates. To ensure that our analog studies are relevant to presolar SiC grains in Wild 2, we focused on craters originating from the impact of submicron refractory grains, but also included some larger craters (4–11 μm) to observe any changes in properties as a function of crater–projectile size. FIB of such small structures typically only allows extraction of a single cross section, from which to measure the surviving grain diameter. To maintain consistency, each section was taken near the crater's center. However, if the impacting grain remnants are not placed symmetrically within the crater, this two-dimensional TEM observation may not sample the full cross sectional width of the grain, and this will add some uncertainty to our measurements, especially for those larger craters which showed fragmented surviving grains with nonuniform distribution of material. TEM examination using a JEOL 2000FX and a JEOL 2100F (both equipped with energy dispersive X-ray spectrometry) permitted determination of the grain morphologies, crystal structures, and chemical compositions. The lattice parameter determinations for the impacting phases were calibrated by assuming a 4.05Å spacing for diffraction spots from α-Al. Distinguishing between TiN (FCC; 4.24 Å) and TiC (FCC; 4.35 Å) was occasionally difficult; both have very similar crystal structures and low energy peaks (such as N and C), and are often weak and sometimes buried in the low energy background especially for thicker sections. In ambiguous cases, the phase is listed as TiC/TiN; however, for practical purposes the two phases are quite similar in density, melting temperature, and other key parameters.

As the depths and diameters of craters can be related to the density and size of the impactors (Kearsley et al. 2007; Price et al. 2010), calibrations were performed in the SEM, FIB, and TEM to ensure that all distance measurements were correct within ~5%. The crater diameters were measured from center to center of the raised crater lip, consistent with the method of Kearsley et al. (2006). The lip-to-lip diameter is often ~15–20% larger than the interior diameter (measured between interior crater walls at the plane of the original Al foil surface) for larger craters, but the two diameters are more similar for small ones which often do not have an appreciable raised crater rim. Crater depths were measured from the foil surface down to the top surface of any surviving crystals in FIB cross sections. Depth determinations from stereometric reconstructions (i.e., using Alicona MEX; Kearsley et al. 2007) were found to be unreliable for the smaller craters of this study.

To test our ability to accurately measure surviving material at the bottom of small craters, secondary ion mass spectrometer measurements using NanoSIMS were made on a different subset of 10 Si-rich and 6 Ti-rich craters using either ^{12}C,^{13}C, $^{12}C^{14}N$, ^{28}Si, and ^{30}Si, or ^{12}C,^{13}C, $^{12}C^{14}N$, $^{12}C^{15}N$, and ^{28}Si in imaging mode. The craters ranged from 0.3 to 8.5 μm in diameter, and again were likely formed by single grain impacts of SiC, Si_3N_4, TiC, and TiN projectiles (i.e., they were similar to grains studied by FIB–TEM). The raw projectile materials (including SiC, Si_3N_4, TiC, and TiN grains) and a Si wafer were used as standards for C, N, and Si isotopic ratios.

Table 1. Summary of crater size from SEM and TEM results on surviving projectile grains for the set of Ti-rich and Si-rich craters studied (listed in order of crater size).

Crater name	Crater diameter (μm)[a]	No. of surviving grains	Surviving grain size (nm)[b]	Avg. aspect ratio[c]	Phase
Si3	0.9	1	525	0.7	SiC
Ti4	1.0	1	325	1.8	TiN
Ti3	1.6	2	270–330	0.7	TiN
Si2	1.7	1	510	1.0	Si_3N_4
Ti5	2.5	3	80–400	0.8	TiC/TiN[d]
Ti6	5.2	2[e]	330–450[e]	0.6	TiC
Si1	5.2	2	200–250	0.7	SiC
Ti9	5.4	3	580–720	0.5	TiC/TiN[4]
Ti7	5.6	6	240–580	0.7	TiN
Ti1	5.7	5	115–425	0.8	TiC/TiN[4]
Ti8	7.1	2	520–880	0.5	TiC
Si4	11.4	6	300–550	0.8	SiC

[a]Lip-to-lip diameter measured from centers of raised crater rims (i.e., Kearsley et al. 2007).
[b]Size range indicated if crater contains multiple crystalline fragments.
[c]For the aspect ratio calculation, the numerator is the dimension perpendicular to foil surface and the denominator is parallel to it (i.e., flattened grains have aspect ratio less than unity).
[d]In these cases, chemical and structural data could not distinguish between isostructural TiC and TiN.
[e]Damage during FIB section preparation makes result uncertain.

RESULTS

To determine the morphology, phase, and microchemistry of surviving material at the bottoms of the craters, we prepared FIB–TEM sections from four Si-rich and eight Ti-rich craters. We found significant amounts of surviving crystalline material at the crater bottoms, and these refractory crystals are often surprisingly well preserved. Table 1 summarizes the crater diameters and the TEM observations on surviving grains found at the bottom of crater FIB sections, including the number of surviving crystalline fragments at the crater bottom, their sizes, their aspect ratios (average value listed in cases of multiple fragments), and their crystal structures when available. The number of crystalline fragments and their aspect ratios (reported with the numerator measured parallel to the foil plane and denominator perpendicular) indicate the degree to which the projectile was fragmented and/or flattened on impact: aspect ratios of less than 1 indicate some flattening on impact (e.g., by partial melting). Our results demonstrate the intact survival of grains of all Ti- and Si-rich refractory phases and in some cases, this occurs without fragmentation or flattening, especially for smaller projectiles. The phase determinations show that the projectiles have the same crystal structures before and after impact. Larger impactors tend to be broken into smaller fragments and are more flattened: the average aspect ratio of >5 μm-sized craters is 0.6, whereas that of craters <5 μm is 1.0. Although NanoSIMS measurements of Stardust craters have detected presolar grains mostly in the raised rims of larger craters (Floss et al. 2013), we found no surviving projectile material in the rims. We now present microstructural details of the surviving grains, which along with Table 1 reveal properties and trends relevant to interpretation of Stardust samples.

Si-Rich Craters

Three analog craters (Si1, Si3, and Si4; Figs. 1a, 1c, and 1d) establish that crystalline SiC can survive a Stardust-like impact into Al foil. Most remarkable is the Si3 crater of ~900 nm diameter, which contains a ~500 nm diameter SiC at its bottom is of a typical size for a presolar SiC (Daulton et al. 2003). Figure 1g shows the surviving SiC crystal at the bottom of the Si3 crater imaged at the [112] orientation along with the corresponding 3C-SiC diffraction pattern and a schematic showing the crystal's size and shape. The grain shape is visible in the image (darker than the surrounding Al regions but lighter than the Pt-filled crater above), and this shape was confirmed with spot EDX and microdiffraction patterns. The large size of the crystalline grain relative to the crater suggests that the entire projectile survived impact intact, based on comparison of the crater diameter to projectile diameter ratio with those of Price et al. (2010). Crater Si1 with 5.2 μm diameter contains two relatively small SiC fragments (200–250 nm in diameter at the crater bottom. Figure 1e shows the Pt-filled Si1 crater with arrows indicating the positions of the two SiC fragments; an inset image of the left SiC shows this faceted crystal at its [112] orientation. The [101], [114],

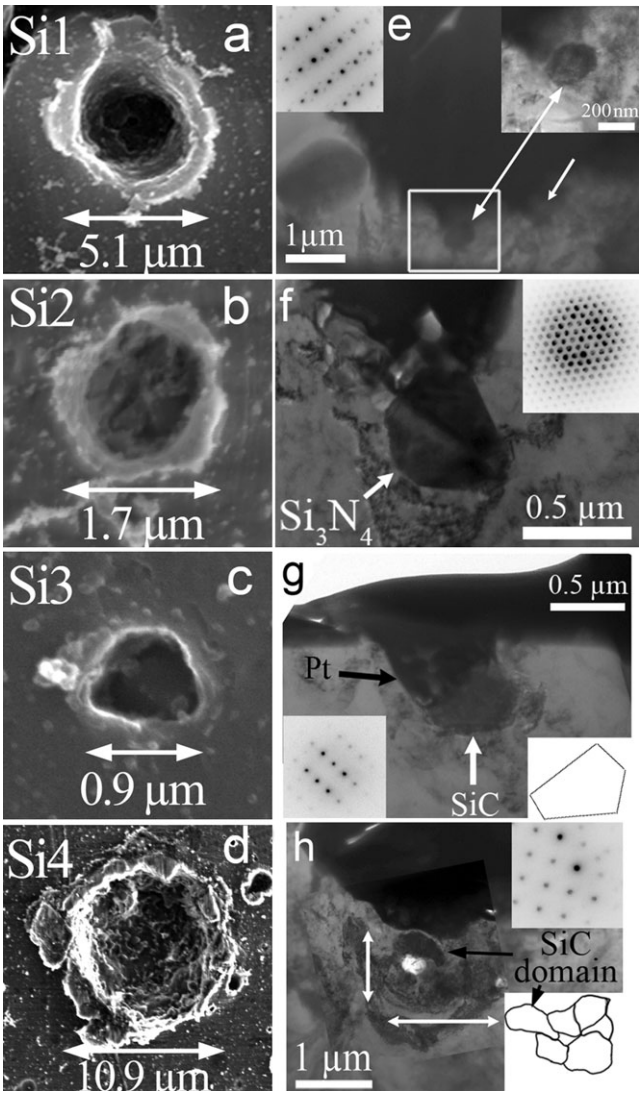

Fig. 1. a–d) Secondary electron images of Si-rich craters Si1, Si2, Si3, and Si4 with lip-to-lip diameter labeled, and bright-field TEM images of: e) Si1 crater cross section with positions of two fragments indicated by white arrows and inset images of a SiC grain and its 3C-SiC [112] diffraction pattern, f) large-faceted Si_3N_4 grain at bottom of Si2 crater with [0001] diffraction pattern, g) SiC grain (645 × 430 nm) at bottom of Si3 crater with inset 3C-SiC [112] diffraction pattern and schematic drawn to scale showing the crystallite size and shape, and h) cluster of surviving SiC crystals at bottom of large Si4 crater with schematic showing to-scale size and shape of surviving fragments and [001] 3C-SiC diffraction pattern of domain indicated by arrow.

and [001] diffraction patterns from this 3C-SiC grain were also found, and showed evidence of twinning (faint extra satellite spots around the stronger ones). The microstructure suggests that larger projectiles (>1 μm) tend to fragment on impact but remain crystalline, whereas smaller submicron projectiles can survive intact. Smaller craters such as Si3 (Fig. 1c) also tend to lack prominent raised crater rims of the type seen on the Si1 crater (Fig. 1a). The FIB section of the ~11 μm diameter Si4 crater contains a clump of surviving SiC grains at its bottom. Six different crystalline domains with diameters ranging between 300 and 550 nm are found in the clump (see to-scale schematic in Fig. 1h), and diffraction patterns from these domains are consistent with the 3C-SiC polytype. The SiC grain boundaries are not clearly distinguishable from the Al at any random orientation, due to similar mass and thickness, but can be seen at high-symmetry crystal orientation due to diffraction contrast; Fig. 1h shows one of the SiC domains (dark in image) at its [001] orientation. Overall, the clump of surviving SiC grains (indicated by white arrows in Fig. 1h) is flattened, and may have undergone plastic deformation on impact or even partial melting. It is unknown whether the impactor originally consisted of these multiple crystalline domains or if this occurred as a result of impact.

That submicron crystalline projectiles can survive intact is reinforced by results from the Si2 crater (Fig. 1b). Here, a relatively large ~500 nm surviving Si_3N_4 crystal is found at the bottom of a ~1.7 μm crater; Fig. 1f shows this faceted grain at its [0001] orientation. Diffraction patterns, including the major [0001] and [−12−16] zones, identify the crystal structure as the common trigonal Si_3N_4 alpha phase. The crystal is still faceted, showing the crystal faces of all three {1010} planes across the top and right side of grain, and does not appear to be flattened. Silicon nitride is the least refractory of the phases in this study, with a melting temperature of 1900 °C, so its well-preserved condition suggests that the peak temperatures and pressures achieved in small crater impacts are sufficiently low to allow intact survival of many refractory grains.

Ti-Rich Craters

Like the Si-rich craters, FIB–TEM sections from Ti-rich craters also showed surviving crystalline material at the crater floors, with minimal material in the crater walls and none on any of the raised rims. Figure 2a shows adjacent Ti-rich craters (Ti4 and Ti5) both formed by submicron TiN impactors that were extracted as a single FIB section. As with Si3, the smaller Ti4 crater lacks the bright surrounding rim of raised material seen around the Ti5 crater. The Ti4 crater shows a single 450 × 230 nm crystalline grain (Fig. 2c) with an inset diffraction pattern that matches the [112] zone of TiN (FCC; $a = 4.28$Å). EDX point spectra taken within the single Ti3 grain show Ti and N along with stray Al and Cu counts from the

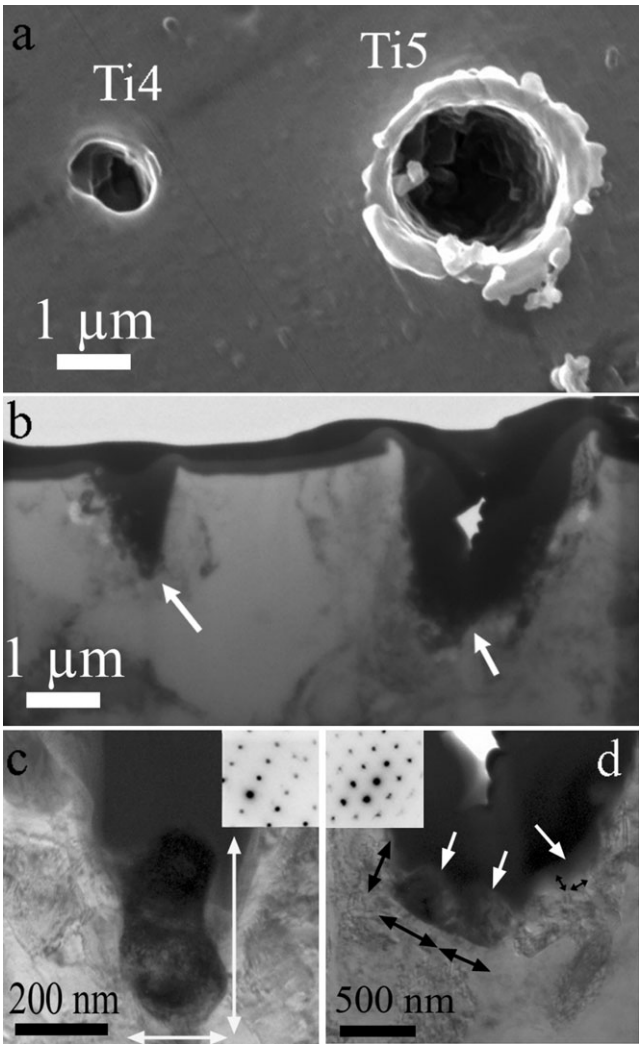

Fig. 2. a) SEM image of adjacent Ti4 and Ti5 craters; b) TEM image of FIB section containing both craters, with dark Pt-filled cross sections and position of surviving grains at the bottom indicated by arrows; c) surviving TiN projectile (450 × 230 nm) at Ti4 crater bottom with long axis perpendicular to Al foil and; d) surviving elliptical TiN projectile with two larger fragments on the crater floor and a small fragment in the crater wall (positions indicated by white arrows and grain dimensions with black ones).

background, whereas no Ti was detected outside of the grain. The Ti4 surviving crystalline grain has an ellipticity of ~1.8, and retains this elliptical shape even after an impact with its long axis perpendicular to the foil. Thus, it was not significantly modified by the impact and clearly did not partially melt and recrystallize on the crater floor nor did it undergo plastic deformation. This is consistent with previous reports of recovery of unmelted wollastonite after impacts in aluminum foil at 6 km s^{-1} (Wozniakiewicz et al. 2012b). The slightly larger Ti5 crater (Figs. 2b and 2d) also shows surviving TiN crystallites (indicated by white arrows in Fig. 2d), although in this case three separate crystalline fragments were found (two ~400 nm diameter grains at the bottom and a ~80 nm one along the side wall). Diffraction patterns from all fragments were consistent with the [011] fcc phase (a = 4.16Å) and EDX spectra are consistent with TiN. The Ti4 projectile impacted with its major axis perpendicular to the floor, resulting in a more carrot-like crater shape relative to Ti5 (Fig. 2b). The crater depth-to-diameter ratios are 1.0 and 0.9 for Ti4 and Ti5, respectively and the crater cross section diameter is reduced to 42% of the full diameter at half height in carrot-shaped Ti4, as opposed to 85% in the more bulbous Ti5 crater. The TiN projectiles that created the Ti4 and Ti5 craters both impacted into the same large single crystal of α-Al (as determined by TEM), so the observed differences in crater shape are not due to any properties of the Al foil (e.g., crystal orientation of the target). Thus, the depth of a given crater is not only a function of density (i.e., depth increases with diameter as seen in fig. 2 of Kearsley et al. [2007]) but can also depend on the impact angle of elliptical projectiles. Such behavior has also been seen for wollastonite impactors (Wozniakiewicz et al. 2012b); see Burchell and Mackay (1998) for a discussion of crater shape for normal incidence of nonspherical impactors.

Larger Ti-rich craters (>5 μm) again tend to have multiple surviving crystal fragments. Figure 3 shows the ~6 μm diameter Ti1 crater, its FIB cross section, and surviving TiN crystals at the crater bottom. The original projectile is broken into five crystalline fragments which are apparently somewhat flattened on impact (average aspect ratio of 0.8). The inset diffraction pattern is identified as an [011] zone axis of an fcc crystal (a = 4.17 ± 0.05 Å) which, along with detectable N-K intensity, shows a TiN crystal. Figure 4a shows the Ti7 crater with six surviving crystalline fragments strewn across the crater floor. Diffraction patterns from one fragment are chemically and structurally consistent with TiC (FCC; a = 4.35 Å) and all fragments are crystalline. Figure 4b shows the Ti9 crater, which has two larger surviving crystalline clumps, both of which are structurally and chemically consistent with TiN. In all the Ti-rich large craters (Ti1, Ti7, and Ti9), the fragments are flattened in the direction of impact and do not show faceting to the same extent as seen in smaller craters. This is also true of other surviving crystalline grains in larger Si- and Ti-rich craters (>4 μm), which show an average ellipticity of 0.65 in comparison to the smaller ones, which have an average ellipticity of 1.0. Figures 4c and 4d show SEM images of the Ti7 and Ti9 craters overlaid with the Ti X-ray intensity of line profiles across the craters, which are derived from spectral images. The Ti X-ray line profiles

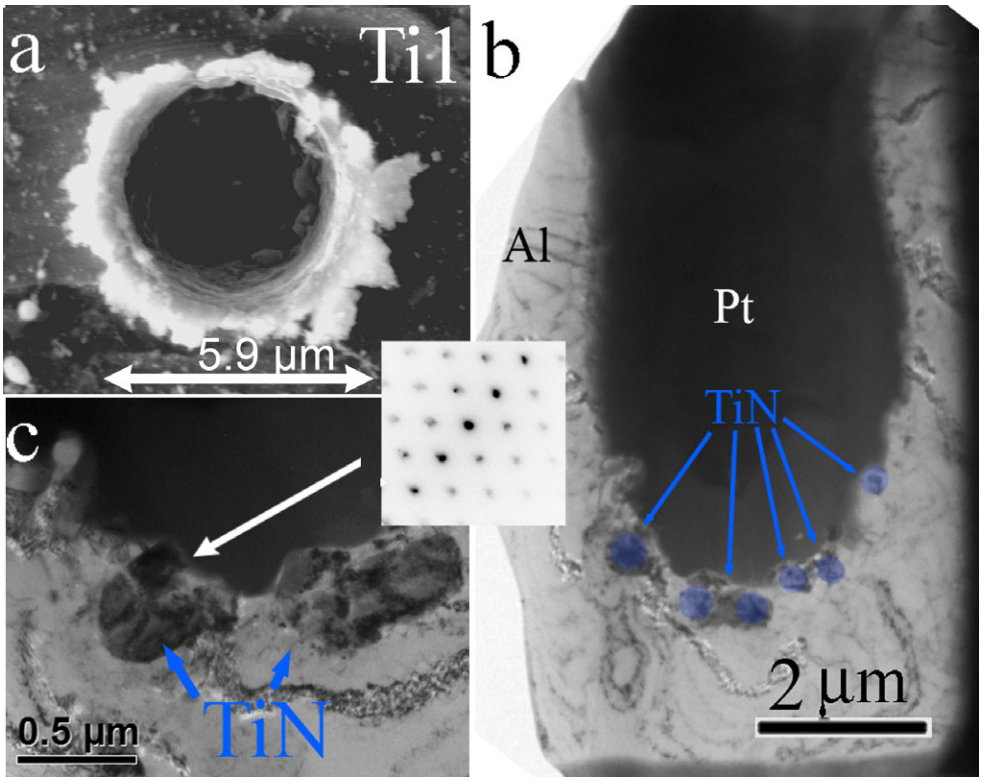

Fig. 3. a) SEM image of Ti1 crater with lip-to-lip diameter indicated, b) TEM image of Ti1 crater FIB cross section showing a dark Pt-filled crater with multiple TiN crystalline fragments at the crater's bottom, and c) close-up TEM image of two largest TiN crystalline fragments with inset [011] fcc diffraction pattern from left fragment.

from spectral images match well with the grain positions in the respective FIB sections: the Ti9 line profile shows two peaks which is consistent with the two separate TiN fragments in Fig. 3b and the Ti7 profile shows higher Ti intensity at the right side of the crater which is consistent with the location of most of the TiC fragments in Fig. 3a. Thus, spectral images can provide decent approximations of the spatial distributions of surviving projectile/impactor material. Though we only have FIB results from 12 craters, the tendency toward fragmentation of larger projectiles (relative to the intact smaller ones) is reinforced by spectral images that were taken from an additional 50 craters over a range of crater diameters.

Crater–Projectile Size Relationships

A primary purpose of producing analog foil impacts has been to determine the dependence of quantifiable crater characteristics (such as crater size, shape, and chemical composition of surviving grains) upon the nature of the impacting material. Such knowledge allows development of useful classifications for individual Stardust craters, thence allowing one to focus detailed but time-consuming FIB–TEM studies on specific subsets of interesting cometary grains. Earlier analog crater studies of various materials established relationships between the size and shape of the Al crater and the type of projectile that created it. As the physical crater properties can be measured quickly and nondestructively, such relationships can be used together with chemical information to estimate the density, size, and chemistry of the impactor. Kearsley et al. (2007) showed that for impacts of relatively large (>10 μm) silicate particles at the same velocity and onto the same target, the crater diameter is typically a fixed multiple of the impactor diameter. The relationship is also density-dependent, and the depth-to-diameter ratio of the crater is related to the impactor density. Although micrometeoroid impacts into Al did receive considerable attention during analyses of the LDEF mission (e.g., McDonnell et al. 1993), due to sample preparation difficulties before the advent of FIB extraction, most of those studies focused on craters considerably larger than the type considered here. In a detailed study of smaller craters more comparable to those reported here, Price et al. (2010) found significant changes to these relationships for smaller impactors (<10 μm diameter). While the small refractory projectiles from our study were not fired as a

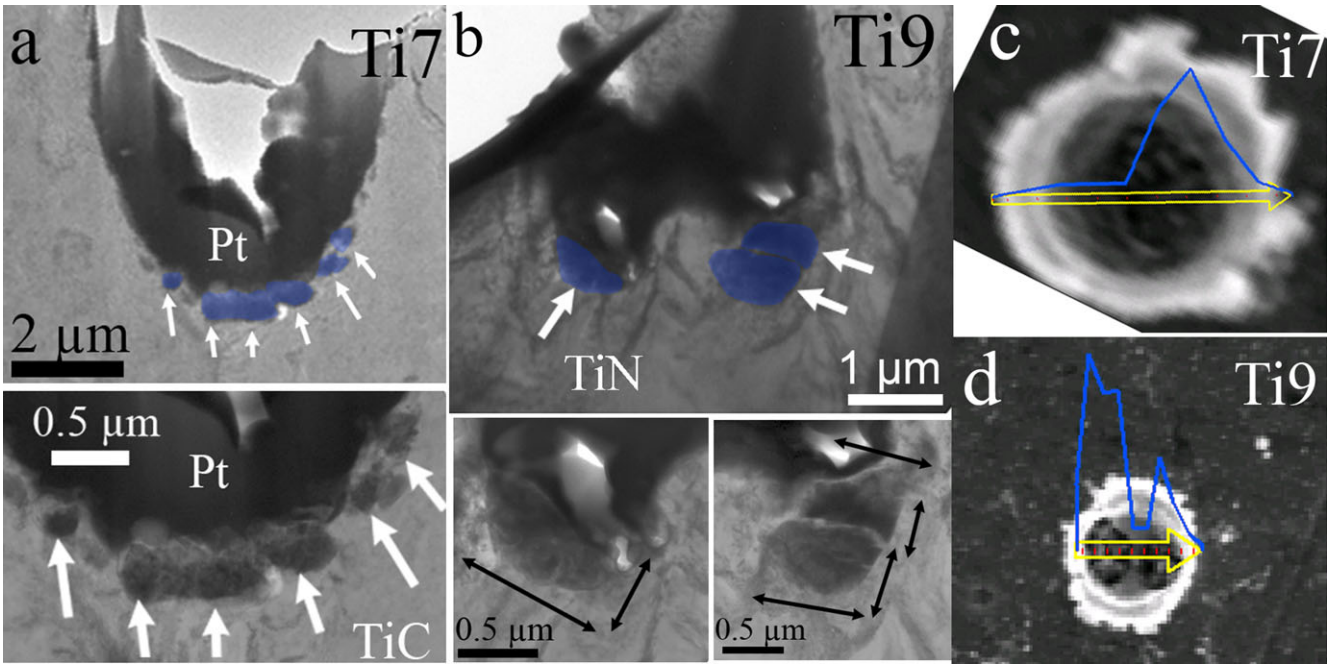

Fig. 4. a) TEM image of entire Ti7 Pt-filled crater cross section (with TiC grains shaded in blue) and close-up TEM image of surviving TiC fragments strewn on crater floor (positions indicated with white arrows); b) TEM image of Ti9 crater cross section and close-up images of both grain-containing regions with dimension of surviving TiN grains indicated with black arrows; and c and d) SEM images of Ti7 and Ti9 craters (respectively) with line profiles of Ti X-ray intensities extracted from spectral images that reflect the observed spatial distributions of Ti-rich grains.

monodispersed powder, their size distribution is known from prior TEM studies, which then allows us to also evaluate the crater-to-projectile size relationships.

Estimates of the impacting grain size derived from observed crater size are particularly useful for assessing the feasibility of certain SIMS measurements. For grains with densities ranging from 3.2 for SiC to 5.4 g cm^{-3} for TiN, the impacting grain diameters are predicted to be 5–6× smaller than the crater diameters based on studies of 10–100 μm silicate projectiles (fig. 7 from Kearsley et al. 2007). Subsequent studies of 0.5–10 μm silica projectiles by Price et al. (2010) have shown agreement with Kearsley et al. (2007) at larger diameters, but show a transition toward smaller multipliers for projectiles <2.4 μm (i.e., the crater is only ~1.6× larger than the projectile instead of 4.6×; see fig. 3 in Price et al. 2010). If we assume that most of the projectile survives impact and is embedded at the crater bottom, we can estimate its original size based on the material found in the FIB cross section.

As the surviving grains are often significantly larger than would be expected based on the crater diameters (i.e., 1.6× multiplier and not 4.6×), the assumption of minimal material loss on impact is sound. Single intact surviving grains are consider to be ellipsoids, with width (a) and height (c) measureable from TEM cross section (and an assumed depth $b = a$). A single effective diameter is then reported for each projectile from this ellipsoidal volume as if the original projectile were equant ($a = b = c$). For craters with multiple crystalline fragments, each fragment is considered ellipsoidal and resulting volumes are summed prior to determining a single effective diameter, and in such cases, fragmentation can lead to underestimation of the original projectile's size. For our small craters (<2.5 μm), we estimate that the impacting grain diameters ranged from 0.4 to 0.8 μm and, thus, the crater diameters are 2.4× (±0.7×) larger that the estimated projectile diameters. These are in good agreement with the Price et al. (2010) results after taking the higher density of our projectiles into account. For the larger craters (5–11 μm) with fragmented surviving grains, determinations of the original impactor size are too uncertain to allow evaluation of the crater size to impactor size relationships. Our results confirm that crater diameters are a smaller multiple of the projectile diameter for submicron refractory impactors. Such changes in cratering behavior have been attributed to increased strain rate hardening for submicron impacts and to changes in strength to strain behavior when projectiles are smaller than the typical sizes of the grains that comprise the Al foil (Price et al. 2010).

The depth-to-diameter ratio of an Al foil crater is related to the density of the impacting phase (Kearsley

et al. 2007), with denser phases creating deeper craters. Thus, one can use stereo pair images to create digital elevation models, which reveals the approximate density of the impacting grain. Based on analog studies of >10 μm projectiles (e.g., fig. 3 in Kearsley et al. 2007), the depth-to-diameter ratios from SiC, Si_3N_4, TiC, and TiN impactors (whose densities range from 3.2 for SiC to 5.4 g cm^{-3} for TiN) are expected to range from 0.57 to 0.72 with increasing density. Our FIB–TEM results show that the less-dense Si-rich phases (Si1 to Si3) have an average depth/diameter ratio of 0.55, in good agreement with these projections. The denser Ti-rich phases have depth/diameter ratios of 0.97 ± 0.09 (excluding two outliers), which is somewhat deeper than the 0.7 value predicted based on fig. 3 of Kearsley et al. (2007). The low outlier Ti3 is probably erroneous due to a noncentral FIB section. The Ti1 crater has a depth-to-diameter of 1.8, and such variations may be caused by impact of elliptical grains. Our observations show the expected increase in depth/diameter with increasing density, and thus suggest that depth-to-diameter relationships are a valid method that can aid in distinguishing between low and high density impactors in Stardust Al foil samples.

NanoSIMS of Analog Craters

To ensure that the low presolar grain abundances measured in Stardust foils (Stadermann et al. 2008; Floss et al. 2013) are not caused by an inability to accurately measure the material in the bottom of Al foil craters, NanoSIMS isotopic measurements of C, N, and Si were made from 14 small analog craters, ranging from 0.3 to 8.5 μm in diameter. Useful secondary ion yields of C and Si from SiCs at the bottom of craters were consistent with expectations for NanoSIMS (~1%), showing that the crater topology did not adversely impact our ability to measure them. No significant variations were seen in the $^{28}Si/^{30}Si$ or $^{12}C/^{13}C$ ratios from the solar values. The $^{14}N/^{15}N$ ratios did vary by ~10% across different samples, suggesting that this ratio (which is measured with the CN− molecular ion) is more sensitive to changes in sample topology. These results demonstrate that if an intact presolar SiC were present at the crater bottom, it should be detectable using standard NanoSIMS methods (e.g., Floss et al. 2013). Clear differences in N/C count ratios were evident among the Si-rich craters ($N = 8$); N-rich craters (presumably Si_3N_4) had $N/C = 3.5 \pm 0.8$, whereas N-poor ones (presumably SiC) showed $N/C = 0.5 \pm 0.2$; similar N variations were seen among the Ti-rich craters ($N = 4$). Thus, for these samples one can differentiate between the C-rich and N-rich grains using SIMS alone. N count rates were 4× higher from Si_3N_4 craters than for TiN ones, but such variability in ion yields between different phases is not unusual.

DISCUSSION

Survival/Condition as Function of Crater (and Impactor) Size

Our analog test shot results on Ti- and Si-rich carbides and nitrides show that submicron refractory grains can survive Stardust-like impacts into Al foil. Many of the grains are preserved in sufficiently good condition to allow chemical and structural investigations that adequately reflect their properties prior to impact. In particular, SiCs of a size comparable to most presolar SiCs should survive intact in small craters. This is most evident in the preservation of the elliptical TiN after an impact with its long axis perpendicular to the foil surface (Fig. 2c). Even the least-refractory Si_3N_4 grains survive and retain their crystal faces (Fig. 1f) rather than having rounded faces characteristic of a resolidified melt. This is consistent with the previous reports of recovery of crystalline fragments of larger (>20 μm) mineral projectiles in impacts on aluminum at 6 km s^{-1} (see Burchell et al. 2008b), wherein Raman spectroscopy confirmed that surviving crystalline material was present. In that article, Raman spectroscopy was conducted on the fragments indicating the presence of crystalline material in the residue, and their unmelted nature was implied by survival of rod shaped fragments of wollastonite whose orientation was aligned with the main axis of an elliptical crater, a result confirmed by TEM analyses (Wozniakiewicz et al. 2012b). Similarly, Foster et al. (2013) studied residues of 10–12 μm olivine grains after impact and again confirmed presence of surviving crystalline material with Raman spectroscopy. However, they also reported significant shifts in the olivine Raman peaks which were attributed to significant strain in the samples postimpact. While they remained crystalline, all of these larger (>10 μm) impactors experienced fragmentation on impact of the type seen in the larger impactors of this study, and such observations of distorted captured grains helps explain the Raman shifts.

The vast majority of the surviving crystalline material was found in the crater bottom, with little material in the crater walls or rim. Our SIMS results on SiC analogs show that there are no intrinsic problems that hinder our ability to isotopically measure such grains in the bottoms of 1–10 μm craters. These results, namely the intact survival of grains at the crater bottom and the ability to measure them, are not in agreement with presolar grain abundances from the Stardust Wild

2 craters (Stadermann et al. 2008; Floss et al. 2013). Those NanoSIMS studies showed very low abundances of presolar grains, and in the four cases where such grains were found, all were in the raised crater rims. However, those studies were predominantly made on larger craters (30–300 μm diameters) and thus our observations of submicron impactors may not be directly comparable. In addition, while many presolar oxides (such as spinel, corundum, and hibonite) and some silicates (such as crystalline forsterite) are comparably refractory to Si_3N_4, many presolar silicates are less refractory, and thus again our observations may not be directly comparable.

Grain Condition Dependence on Impactor Size

A hint at a possible resolution of the inconsistencies between our small crater results and the SIMS studies of mostly larger (30–300 μm) craters (e.g., Stadermann et al. 2008) comes from observed changes in the condition of surviving crystallites as a function of impactor-crater size. Crystalline grains in >5 μm larger craters (e.g., Ti1, Ti7, and Ti9 craters) were fragmented and somewhat flattened on impact, and aspect ratios of grains from large >5 μm craters were considerably lower than those of smaller craters. The flattening of larger projectiles of the same phases due to partial melting and/or plastic deformation suggests an increase in the peak temperatures and pressures to which they were subjected. This transition in the observed behavior of projectiles as a function of size coincides with a transition in the projectile size to crater size relationship near this crater diameter (fig. 3 of Price et al. 2010), wherein the projectiles in <2 μm craters create craters that often lack a raised rim (e.g., Si3 in Fig. 1c and Ti4 in Fig. 2a).

Impact Pressures

The peak shock pressures for a range of mineral grains (augite, anorthsite, basalt, dunite, olivine, and spinel) impacting Al foil at 6.1 km s^{-1} were reported in Burchell and Kearsley (2009). Using the planar impact approximation (PIA), the estimate peak shock pressures ranged from 60 to 90 GPa, depending on the mineral. If one uses the same approximation for SiC (assuming a SiC density of 3020 kg m^{-3} and, based on data in the LASL wave speed database, a linear wave speed relation for SiC with C and S constants of 7.092 and 1.049 m s^{-1}, respectively), we find that at 6.05 km s^{-1}, the estimated peak shock pressure for SiC is 79 GPa for a 6.05 km s^{-1} impact speed. In terms of impact metamorphism, this is normally taken as sufficient not just to cause fragmentation of the impactor but also the onset of melting. It should be noted, however, that the PIA applies to the case of contact between two semi-infinite planes, whereas here the projectiles are finite in size. As noted by Price et al. (2010); for impacts by projectiles of less than 10 μm, the small size of the projectiles increases the strain rate sufficiently such that the strength of the Al target increases significantly, thus increasing the peak shock pressures. It should also be noted, however, that these peak pressures apply near the contact plane and the bulk of the impactor will be shocked to a lower pressure (Pierazzo and Melosh 2000). The role of cold Al as an extraordinarily effective heat sink may, however, also contribute to dampening of postshock thermal alteration in the smallest grains. This is in marked contrast to silica aerogel, whose extraordinarily low thermal conductivity may retain sufficient heat to allow prolonged thermal processing of finer material.

Implications for Presolar Grain Abundance Determinations in Wild 2 Stardust

About ~95% of the measurement areas for the Wild 2 presolar grain abundance determinations were from >30 μm craters (size range of 30–300 μm; Floss et al. 2013), and any surviving material may thus have been subjected to higher peak temperatures, leading to more intense modification. The isotopic anomalies associated with any presolar grains in these craters would become diluted during the collision through isotopic exchange with the surrounding partially molten material (i.e., scenario 3 of fig. 9 in Floss et al. 2013). This presolar grain destruction via diffusion of anomalies would be further magnified for presolar silicates, which are considerably less refractory than SiC. The presence of some surviving presolar grains in raised crater rims suggests less extreme T and P or more rapid cooling in these regions (in comparison to the bottom of craters), which allows for retention of their isotopic anomalies.

Our results suggest that the survival of a typical ~500 nm presolar SiC grain (Amari et al. 1994) may depend on whether it impacts alone as a single grain in a small (≤1 μm) Al foil crater, or whether it impacts as part of a larger aggregate of material in a large crater. Presolar grains that impact as larger aggregates can experience multiple phases of compressive shock that lead to higher peak temperatures relative to single grain impactors (e.g., Wozniakiewicz et al. 2012a). Presolar grain abundance estimates based on large craters may therefore be inaccurate (Floss et al. 2013) due to isotopic dilution on impact. However, the intact condition of SiC in small craters suggests that more accurate presolar grain determinations can come from NanoSIMS measurements of small craters, which is the

approach taken by Leitner et al. (2010, 2012). They estimate the abundance of O-rich presolar grains in small Stardust craters as ~1100 ppm, although with high uncertainties due to finding only one O-rich presolar grain among ~1000 crater measurements. This estimate is somewhat higher than the corrected estimate of 600–800 ppm from the large crater SIMS measurements (Floss et al. 2013). However, the accuracy of the small crater approach will be limited by the laborious nature of locating and measuring thousands of small craters in the NanoSIMS.

Microstructural Studies of Stardust Al Foil and Aerogel Samples

In addition to providing insights into presolar grain abundances, the intact survival of grains in small craters has other implications for Stardust Wild 2 research. In particular, FIB–TEM of such grains can provide a complementary means to study the Stardust fine fraction. To assess the applicability of such studies, it is useful to compare our results from refractory analogs with some of the actual samples from the Stardust mission. Over 500 small craters have been investigated with EDX (Price et al. 2010), and in ~35% of them, the elements detected allow conclusive identification of the impacting grain. Of those identifiable grains, ~20% were Mg or Fe silicates, ~20% were sulfides, and ~40% were mixtures of sulfides and silicates, and only ~2% were Si-dominated (Price et al. 2010; Stroud et al. 2010). FIB–TEM studies of 22 Al foil craters in the 1–3 μm size range have been reported (Leroux et al. 2008, 2010; Stroud et al. 2010), and these are predominantly consistent with impacts of submicron olivine, pyroxene, and Fe-rich sulfides or aggregate of these, which is consistent with the EDX survey. Many of the less-refractory grains are rendered amorphous by the impact or suffer from shock metamorphism. However, relatively large intact crystals like those we report are found in some cases (e.g., enstatite in crater 2 of Leroux et al. [2008] and chromite in crater b4 of Stroud et al. [2010]), and these reinforce the fact that surviving crystalline grains are also present in the Stardust cometary foils. The thin layers of surviving melt in some craters (e.g., craters 1, 4, and 7 of Leroux et al. 2008) make it clear that less-refractory phases will undergo major modification on capture and that intact, crystalline grains are not the typical result of capture in Al foils. We are currently investigating the extent of such modifications on capture for other fine-grained common meteoritic materials using the Acfer 094 analog test shots.

Our expectations of what surviving grains will be found in FIB–TEM crater studies are shaped by earlier studies of aerogel-captured Wild 2 grains. Most studies thus far have concentrated on the larger terminal particles (typically ~10 μm diameter) found at the end of aerogel tracks (e.g., Joswiak et al. 2012). These particles are comprised of both single mineral fragments (mostly olivine and enstatite) and also rock fragments of various types including chondrule fragments. However, this coarse fraction of captured grains may be a different population from the fine ones that form small craters. The many fine grains found in aerogel track walls have received less attention, but these can also be studied with TEM after they are compressed, embedded, and ultramicrotomed. Stodolna et al. (2012) carried out a comprehensive TEM study of ~500 smaller grains found in the walls of track 80. Mineral fragments (~1 μm in diameter) were present, predominantly silicates such as olivine and pyroxene, along with a considerable amount of GEMS-like material (silica-rich glass with embedded iron metal and metal sulfide beads). However, mixing and melting of fine grains with the aerogel in the track walls complicates the study and interpretation of this material; for example, it has been shown that laboratory impacts of various minerals into aerogel produce GEMS as an artifact of the impact process (Ishii et al. 2008).

The results of this study suggest that chemical composition surveys and subsequent FIB–TEM studies of small craters can give insights of the Wild 2 fine fraction. Rapid X-ray spectrometry crater surveys can quickly reveal the approximate compositions of surviving material, which in turn can guide selection of FIB–TEM targets. Of particular interest are grains with CAI-like compositions which should be sufficiently refractory to survive impact as intact crystals. Even for less-refractory impactors, which will be less well preserved, Al foil samples offer a complementary approach to aerogel-collected samples; concentration of the surviving material at the crater bottom can allow targeted chemical and isotopic measurements without interference from aerogel. It also may be possible to detect craters that contain presolar SiCs through relatively rapid X-ray mapping alone, with a focus on the crater size range (0.5–1.3 μm) that matches the known presolar SiC size distribution (0.3–0.8 μm; Daulton et al. 2003). Such X-ray mapping can detect presolar SiCs in primitive meteorite matrix material, where their Si-rich and Mg- and O-poor compositions are clearly distinct from other matrix components (Bernatowicz et al. 2003). Any such detection would be more complicated if SiC-containing craters also contained fine silicate or sulfide material, as is the case for many submicron craters (Leroux et al. 2008, 2010; Stroud et al. 2010). Such an impact would likely result in an intact crystalline SiC with a thin amorphous layer

containing the sulfide or silicate material. It is possible that rapid X-ray mapping could reduce, by several orders of magnitude, the number of small craters that would need to be measured by SIMS to get an accurate estimate of the presolar SiC abundance.

SUMMARY AND CONCLUSIONS

FIB–TEM studies of Stardust analog craters show that submicron SiC and other comparably refractory phases can survive impact into Al foils. SiC grains survive as intact crystals at the bottom of small craters and often are not flattened on impact, showing no evidence for melting or plastic deformation. Grains of the least-refractory phase considered here (Si_3N_4) also survive as intact, faceted crystals. Moreover, even an elliptical TiN grain was able to survive an impact with its long axis perpendicular to the foil with no evidence of flattening. Taken together, these FIB–TEM results suggest that grains found at the bottom of small Al foil craters present opportunities to make chemical, structural, and isotopic measurements on material that is representative of the original Wild 2 samples.

While the same Ti and Si carbide and nitride phases survive in crystalline form in somewhat larger craters (5–10 μm diameter), these surviving projectiles are more commonly found in multiple fragments strewn across the crater floor and sometimes in the crater walls. Furthermore, the grain fragments are normally flattened in the direction of impact (i.e., no longer equant), indicating greater modification on impact via partial melting or plastic deformation. We confirm the transition seen in the crater-to-projectile diameter relationship as the impactor size decreases below ~3 μm (Price et al. 2010). The smallest (<2 μm) craters formed by impact of single refractory grains and lack the prominent raised rims seen around larger ones, which may bias the detection of craters in this size range using visual or automated crater searches (e.g., Ogliore et al. 2012).

The evidence for greater modification on impact as projectile size increases may explain the low presolar grain abundance for Wild 2 that were derived primarily from SIMS measurement of 50–300 μm diameter craters. The higher peak temperatures reached in larger impacts result in melting and subsequent isotopic dilution of small presolar grains, when these grains impact together as a larger aggregate of material (a scenario proposed by Floss et al. 2013). The only surviving presolar grains found in >50 μm craters were in the grain rims, despite the fact that most material is in the crater bottom, suggesting that only at the crater's perimeter are grains quenched rapidly enough to preserve their isotopic anomalies. NanoSIMS measurements of small Si-rich analog craters showed normal ion yields and sufficient counts to detect small presolar SiCs if present. The survival of grains in the smaller craters (<2 μm) suggests that more accurate presolar grain estimates could result from SIMS measurements of such craters, which is a method pursued by Leitner et al. (2010, 2012).

The relatively pristine condition of the fine grains in small, single grain impact craters shows that Al foil Stardust samples are a complementary way to study the Wild 2 fine fraction without mixing and melting with surrounding aerogel. Rapid nondestructive surveys of small craters with EDX can in most cases determine the dominant elements present in the surviving material at the crater bottom. Thus, one can target FIB–TEM studies on subsets of craters that contain grains of the desired composition and size. Of particular further interest are studies of refractory CAI-like minerals, and these can complement other studies of Stardust aerogel tracks (in which the same types of minerals are found). Moreover, due to their unique Si-rich and Mg-, O-poor compositions, it may be possible to detect craters that contain SiCs based on X-ray spectra alone (similar to the method used by Bernatowicz et al. 2003).

Acknowledgments—This work was made possible by NASA grants NNX10AH07G and NNX14AF22G (C.F.). The University of Kent was supported by a grant from STFC.

Editorial Handling—Dr. Donald Brownlee

REFERENCES

Amari S., Lewis R. S., and Anders E. 1994. Interstellar grains in meteorites: I. Isolation of SiC, graphite, and diamond; size distributions of SiC and graphite. *Geochimica et Cosmochimica Acta* 58:459–470.

Bernatowicz T. J., Messenger S., Pravdivtseva O., Swan P., and Walker R. M. 2003. Pristine presolar silicon carbide. *Geochimica et Cosmochimica Acta* 67:4679–4691.

Brownlee D., Tsou P., Aléon J., Alexander C. M. O. D., Araki T., Bajt S., Baratta G. A., Bastien R., Bland P., Bleuet P., Bort J., Bradley J. P., Brearley A., Brenker F., Brennan S., Bridges J. C., Browning N. D., Brucato J. R., Brucato H., Bullock E., Burchell M. J., Busemann H., Butterworth A., Chaussidon M., Cheuvront A., Chi M., Cintala M. J., Clark B. C., Clemett S. J., Cody G., Colangeli L., Cooper G., Cordier P., Daghlian C., Dai Z., D'Hendecourt L., Djouadi Z., Dominguez G., Duxbury T., Dworkin J. P., Ebel D. S., Economou T. E., Fakra S., Fairey S. A. J., Fallon S., Ferrini G., Ferroir T., Fleckenstein H., Floss C., Flynn G., Franchi I. A., Fries M., Gainsforth Z., Gallien J.-P., Genge M., Gilles M. K., Gillet P., Gilmour J., Glavin D. P., Gounelle M., Grady M. M., Graham G. A., Grant P. G., Green S. F., Grossemy F., Grossman L., Grossman J. N., Guan Y., Hagiya K., Harvey R., Heck P., Herzog G. F., Hoppe P.,

Hörz F., Huth J., Hutcheon I. D., Ignatyev K., Ishii H., Ito M., Jacob D., Jacobsen C., Jacobsen S., Jones S., Joswiak D., Jurewicz A., Kearsley A. T., Keller L. P., Khodja J., Kilcoyne A. L. D., Kissel J., Krot A., Langenhorst F., Lanzirotti A., Le L., Leshin L. A., Leitner J., Lemelle L., Leroux H., Liu M.-C., Luening K., Lyon I., MacPherson G., Marcus M. A., Marhas K., Marty B., Matrajt G., McKeegan K., Meibom A., Mennella V., Messenger K., Messenger S., Mikouchi T., Mostefaoui S., Nakamura T., Nakano T., Newville M., Nittler L. R., Ohnishi I., Ohsumi K., Okudaira K., Papanastassiou D. A., Palma R., Palumbo M. E., Pepin R. O., Perkins D., Perronnet M., Pianetta P., Rao W., Rietmeijer F. J. M., Robert F., Rost D., Rotundi A., Ryan R., Sandford S. A., Schwandt C. S., See T. H., Schlutter D., Sheffield-Parker J., Simionovici A., Simon S., Sitnitsky I., Snead C. J., Spencer M. K., Stadermann F. J., Steele A., Stephan T., Stroud R., Susini J., Sutton S. R., Taheri M., Taylor S., Teslich N., Tomeoka K., Tomioka N., Toppani A., Trigo-Rodriguez J. M., Troadec D., Tsuchiyama A., Tuzolino A. J., Tyliszczak T., Uesugi K., Velbel M., Vellenga J., Vicenzi E., Vincze L., Warren J., Weber I., Weisberg M., Westphal A. J., Wirick S., Wooden D., Wopenka B., Wozniakiewicz P., Wright I., Yabuta H., Yano H., Young E. D., Zare R. N., Zega T., Ziegler K., Zimmermann L., Zinner E., and Zolensky M. 2006. Comet 81P/Wild 2 under a microscope. *Science* 314:1711–1716.

Brownlee D., Joswiak D., and Matrajt G. 2012. Overview of the rocky component of Wild 2 comet samples: Insight into the early solar system, relationship with meteoritic materials and the differences between comets and asteroids. *Meteoritics & Planetary Science* 47:453–470.

Brownlee D. E., Joswiak D., and Matrajt G. 2013. The nature and relationship of coarse and the mysterious fine materials collected from comet Wild 2 (abstract #1719). 44th Lunar and Planetary Science Conference. CD-ROM.

Burchell M. J. and Kearsley A. T. 2009. Short-period Jupiter family comets after Stardust. *Planetary and Space Science* 57:1146–1161.

Burchell M. J. and Mackay N. 1998. Crater ellipticity in hypervelocity impact on metals. *Journal of Geophysical Research* 103(E10):22761–22774.

Burchell M. J., Cole M. J., McDonnell J. A. M., and Zarnecki J. C. 1999. Hypervelocity impact studies using the 2 MV Van de Graaff dust accelerator and two stage light gas gun of the University of Kent at Canterbury. *Measurement Science and Technology* 10:41–50.

Burchell M. J., Fairey S. A. J., Wozniakiewicz P., Brownlee D. E., Hörz F., Kearsley A. T., See T. H., Tsou P., Westphal A., Green S. F., Trigo-Rodríguez J. M., and Domínguez G. 2008a. Characteristics of cometary dust tracks in Stardust aerogel and laboratory calibrations. *Meteoritics & Planetary Science* 43:23–40.

Burchell M. J., Foster N. J., Kearsley A. T., and Creighton J. A. 2008b. Identification of mineral impactors in hypervelocity impact craters in aluminum by Raman spectroscopy of residues. *Meteoritics & Planetary Science* 43:135–142.

Croat T. K., Floss C., Sosothikul S., Stadermann F. J., Kearsley A. T., and Burchell M. J. 2013. FIB-TEM investigations into the condition of refractory presolar phases under stardust-like conditions (abstract #2625). 44th Lunar and Planetary Science Conference. CD-ROM.

Croat T. K., Floss C., Haas B. A., Burchell M. J., and Kearsley A. T. 2014. Survival and condition of micron-scale refractory grains in stardust-analog Al foil craters (abstract #1508). 45th Lunar and Planetary Science Conference. CD-ROM.

Daulton T. L., Bernatowicz T. J., Lewis R. S., Messenger S., Stadermann F. J., and Amari S. 2003. Polytype distribution of circumstellar silicon carbide: Microstructural characterization by transmission electron microscopy. *Geochimica et Cosmochimica Acta* 67:4743–4767.

Floss C., Stadermann F. J., Kearsley A. T., Burchell M. J., and Ong W. J. 2013. The abundance of presolar grains in comet 81P/Wild 2. *The Astrophysical Journal* 763:140.

Foster N. F., Wozniakiewicz P. J., Price M. C., Kearsley A. T., and Burchell M. J. 2013. Identification by Raman spectroscopy of Mg-Fe content of olivine samples after impact at 6 km s-1 onto aluminium foil and aerogel: In the laboratory and in Wild-2 cometary samples. *Geochimica et Cosmochimica Acta* 121:1–14.

Hörz F., Bastien R., Borg J., Bradley J. P., Bridges J. C., Brownlee D. E., Burchell M. J., Chi M., Cintala M. J., Dai Z. R., Djouadi Z., Dominguez G., Economou T. E., Fairey S. A. J., Floss C., Franchi I. A., Graham G. A., Green S. F., Heck P., Hoppe P., Huth J., Ishii H., Kearsley A. T., Kissel J., Leitner J., Leroux H., Marhas K., Messenger K., Schwandt C. S., See T. H., Snead C., Stadermann F. J., Stephan T., Stroud R., Teslich N., Trigo-Rodríguez J. M., Tuzzolino A. J., Troadec D., Tsou P., Warren J., Westphal A., Wozniakiewicz P., Wright I., and Zinner E. 2006. Impact features on Stardust: Implications for comet 81P/Wild 2 dust. *Science* 314:1716–1719.

Ishii H. A., Bradley J. P., Dai Z. R., Chi M., Kearsley A. T., Burchell M. J., Browning N. D., and Molster F. 2008. Comparison of comet 81P/Wild 2 dust with interplanetary dust from comets. *Science* 319:447–450.

Joswiak D. J., Brownlee D. E., Matrajt G., Westphal A. J., Snead C. J., and Gainsforth Z. 2012. Comprehensive examination of large mineral and rock fragments in Stardust tracks: Mineralogy, analogous extraterrestrial materials, and source regions. *Meteoritics & Planetary Science* 47:471–524.

Kearsley A. T., Burchell M. J., Hörz F., Cole M. J., and Schwandt C. S. 2006. Laboratory simulation of impacts on aluminum foils of the Stardust spacecraft: Calibration of dust particle size from comet Wild-2. *Meteoritics & Planetary Science* 41:167–180.

Kearsley A. T., Graham G. A., Burchell M. J., Cole M. J., Dai Z. R., Teslich N., Bradley J. P., Chater R., Wozniakiewicz P. A., Spratt J., and Jones G. 2007. Analytical scanning and transmission electron microscopy of laboratory impacts on Stardust aluminum foils: Interpreting impact crater morphology and the composition of impact residues. *Meteoritics & Planetary Science* 42:191–210.

Kearsley A. T., Borg J., Graham G. A., Burchell M. J., Cole M. J., Leroux H., Bridges J. C., Hörz F., Wozniakiewicz P. J., Bland P. A., Bradley J. P., Dai Z. R., Teslich N., See T., Hoppe P., Heck P. R., Huth J., Stadermann F. J., Floss C., Marhas K., Stephan T., and Leitner J. 2008. Dust from comet Wild 2: Interpreting particle size, shape, structure and composition from impact features on the Stardust aluminum foils. *Meteoritics & Planetary Science* 43:41–73.

Kearsley A. T., Burchell M. J., Price M. C., Graham G. A., Wozniakiewicz P. J., Cole M. J., Foster N. J., and Teslich N. 2009. Interpretation of Wild 2 dust fine structure: Comparison of Stardust aluminum foil craters to the three-dimensional shape of experimental impacts by artificial aggregate particles and meteorite powders. *Meteoritics & Planetary Science* 44:1489–1509.

Kearsley A. T., Burchell M. J., Price M. C., Cole M. C., Wozniakiewicz P. J., Ishii H. A., Bradley J. P., Fries M., and Foster N. J. 2012. Experimental impact features in stardust aerogel: How track morphology reflects particle structure, composition and density. *Meteoritics & Planetary Science* 47:737–762.

Leitner J., Hoppe P., and Heck P. R. 2010. First discovery of presolar material of possible supernova origin in impact residues from comet 81P/Wild 2 (abstract #1607). 41st Lunar and Planetary Science Conference. CD-ROM.

Leitner J., Heck P. R., Hoppe P., and Huth J. 2012. The C-, N-, and O-isotopic composition of cometary dust from comet 81P/Wild 2 (abstract #1839). 43rd Lunar and Planetary Science Conference. CD-ROM.

Leroux H., Stroud R. M., Dai Z. R., Graham G. A., Troadec D., Bradley J. P., Teslich N., Borg J., Kearsley A. T., and Hörz F. 2008. Transmission electron microscopy of cometary residues from micron-sized craters in the Stardust Al foils. *Meteoritics & Planetary Science* 43:143–160.

Leroux H., Kearsley A. T., and Troadec D. 2010. Mineralogy of Wild 2 residues in micron-sized craters from the Stardust Al-foils (abstract #1621). 41st Lunar and Planetary Science Conference. CD-ROM.

McDonnell J. A. M., Deshpande S. P., Niblett D. H., Neish M. J., and Newman P. J. 1993. The near Earth space impact environment—An LDEF overview. *Advances in Space Research* 13:87–101.

McKeegan K. D., Aléon J., Bradley J., Brownlee D., Busemann H., Butterworth A., Chaussidon M., Fallon S., Floss C., Gilmour J., Gounelle M., Graham G., Guan Y., Heck P. R., Hoppe P., Hutcheon I. D., Huth J., Ishii H., Ito M., Jacobsen S. B., Kearsley A., Leshin L. A., Liu M.-C., Lyon I., Marhas K., Marty B., Matrajt G., Meibom A., Messenger S., Mostefaoui S., Mukhopadhyay S., Nakamura-Messenger K., Nittler L., Palma R., Pepin R. O., Papanastassiou D. A., Robert F., Schlutter D., Snead C. J., Stadermann F. J., Stroud R., Tsou P., Westphal A., Young E. D., Ziegler K., Zimmermann L., and Zinner E. 2006. Isotopic compositions of cometary matter returned by Stardust. *Science* 314:1724–1728.

Ogliore R. C., Floss C., Stadermann F. J., Kearsley A. T., Leitner J., Stroud R. M., and Westphal A. J. 2012. Automated searching of Stardust interstellar foils. *Meteoritics & Planetary Science* 47:729–736.

Pierazzo E. and Melosh H. J. 2000. Hydrocode modeling of oblique impacts: The fate of the projectile. *Meteoritics & Planetary Science* 35:117–130.

Price J. C., Kearsley A. T., Burchell M. J., Hörz F., Borg J., Bridges J. C., Cole M. J., Floss C., Graham G., Green S. F., Hoppe P., Leroux H., Marhas K. K., Park N., Stroud R., Stadermann F. J., Telisch N., and Wozniakiewicz P. J. Comet 81/P/Wild 2: The size distribution of finer (sub-10 μm) dust collected by the Stardust spacecraft. *Meteoritics & Planetary Science* 45:1409–1428.

Stadermann F. J., Hoppe P., Floss C., Heck P. R., Hörz F., Huth J., Kearsley A. T., Leitner J., Marhas K. K., McKeegan K. D., and Stephan T. 2008. Stardust in Stardust—The C, N, and O isotopic compositions of Wild 2 cometary matter in Al foil impacts. *Meteoritics & Planetary Science* 43:299–313.

Stodolna J., Jacob D., and Leroux H. 2012. Mineralogy and petrology of Stardust particles encased in the bulb of track 80: TEM investigation of the Wild 2 fine-grained material. *Geochimica et Cosmochimica Acta* 87:35–50.

Stroud R. M., Koch I. M., Bassim N. D., Piccard Y. N., and Nittler L. R. 2010. Structure and composition of comet Wild 2 residues in sub-micron to micron-sized craters (abstract #1792). 41st Lunar and Planetary Science Conference. CD-ROM.

Trigo-Rodríguez J. M., Domínguez G., Burchell M. J., Hörz F., and Llorca J. 2008. Bulbous tracks arising from hypervelocity capture in aerogel. *Meteoritics & Planetary Science* 43:75–86.

Wozniakiewicz P. J., Kearsley A. T., Burchell M. J., Foster N. J., Cole M. J., Bland P. A., and Russell S. S. 2009. In situ analysis of residues resulting from laboratory impacts into aluminum 1100 foil: Implications for Stardust crater analyses. *Meteoritics & Planetary Science* 44:1541–1559.

Wozniakiewicz P. J., Ishii H. A., Kearsley A. T., Burchell M. J., Bradley J. P., Price M. C., Teslich N., Lee M. R., and Cole M. J. 2012a. Stardust impact analogs: Resolving pre- and postimpact mineralogy in Stardust Al foils. *Meteoritics & Planetary Science* 47:708–728.

Wozniakiewicz P. J., Kearsley A. T., Ishii H. A., Burchell M. J., Bradley J. P., Teslich N., Cole M. J., and Price M. C. 2012b. The origin of crystalline residues in Stardust Al foils: Surviving cometary dust or crystallized impact melts? *Meteoritics & Planetary Science* 47:660–670.